Applied Surface Science 255 (2009) 6515–6524

Contents lists available at ScienceDirect

Applied Surface Science

journal homepage: www.elsevier.com/locate/apsusc

Effects of N_2 content and thickness on CrN_x coatings on Mg alloy by the planar DC reactive magnetron sputtering

Yongjing Shi [a,*], Siyuan Long [a], Liang Fang [b], Fusheng Pan [a], Huimin Liao [a]

[a] College of Materials Science and Engineering, Chongqing University, Shazheng Street 174#, Shapingba District, Chongqing 400044, PR China
[b] Department of Applied Physics, Chongqing University, Chongqing 400044, PR China

ARTICLE INFO

Article history:
Received 1 August 2008
Received in revised form 3 February 2009
Accepted 13 February 2009
Available online 23 February 2009

Keywords:
CrN_x coatings
Planar DC reactive magnetron sputtering
Structure evolution
N_2 content
Grain growth
Grain size distribution

ABSTRACT

The CrN_x ($0 < x = N/Cr < 1$) coatings on Mg alloy were prepared by DC reactive planar magnetron sputtering at a mixed atmosphere containing Ar and N_2. The effects of N_2 content and thickness on the CrN_x coatings were characterized by the X-ray photoelectron spectrometry (XPS), X-ray diffraction (XRD) and field emission scanning electron microscope (FESEM). The experimental results show that the N atomic concentration increases exponentially and N1s spectrum shifts downward with the increase in N_2 content ($\varphi(N_2)$), and the deposition rate decreases exponentially. The morphologies evolution of CrN_x coatings shows that the growth structure changes from fibre growth to columnar growth with the increase in $\varphi(N_2)$. Based on evolution of phase and structure, a SZM model is summarized, indicating that the change of structure and phase is consistent; ZT and sub-ZT correspond to $Cr_2N + Cr$ and $CrN + Cr_2N$, respectively. The in-plane mean grain size linearly increases and the Root Mean Square roughness W_{RMS} increases exponentially with coating thickening, and grain size obeys Gaussian distribution.

1. Introduction

The Mg alloy is one of the potential materials due to lighter weight and excellent absorption of vibration in areas of aviation and automobile. Several different techniques have been developed for the surface treatment of Mg alloy, but the coatings deposited by physical vapour deposition are of distinct predominance due to the better adhesive and mechanical property. The binary and ternary Cr-based coatings have successfully been prepared on the Mg alloy by magnetron sputtering, such as AlN, CrN, TiN and AlN/TiN [1,2], to improve the corrosion-resistant and mechanical properties. The quaternary nitride coatings on the Mg alloy were researched by magnetron sputtering, and the carbide occurred as an unstable phase in the $CrN_xO_yC_z$ coatings; furthermore, the CrTiAlN coatings on the Mg alloy exhibited excellent mechanical and tribological properties [3,4].

Nitride coatings of transition metal can provide better protection as an important functional material for the protection of key tools and parts of automotive vehicle due to better mechanical properties and corrosion resistance. Chromium nitride coatings have been prepared on high speed steel and stainless steel by different technologies in a mixed atmosphere, such as reactive magnetron sputtering [5], cathodic arc and electron beam evaporation [6,7], etc. Since the 1980s, mechanical properties of CrN_x coatings had been studied, and Cr_2N demonstrated predominant higher hardness and CrN were provided with better oxidation resistance and lower friction coefficient [8]. The composition and structure of CrN_x coatings depended on N atomic relative concentration, the structure of CrN_x coatings changed from the $Cr_2N + Cr$ to the CrN structure, the coating density gradually increased [9].

Coating growth is a complex process controlled by the interplay of both thermodynamic and kinetic driving forces, and the fundamental factors of the deposition process governing growth and microstructure involve deposition process parameters, and surface crystallographic structure and surface roughness of the substrate. The deposition temperature and sputtering gas pressure compose basic technique parameters, and the incidence angle of deposition flux has an important effect on the coating structure, too. For the metal thicker coating growth, the structure zone model was proposed by Thornton [10,11], which characterized three zones as a function of T/T_m and total pressure for conventional planar magnetron sputtering, where T is the deposition temperature and T_m is the melting pointing of coating materials. Based on pulsed magnetron sputtering, Kelly proposed a novel structure model which expressed the effect of O relative concentration on aluminum oxide coatings [12]. Moreover, abundant ion flux impingement can increase adatom diffusion and reduce the particle contamination. In the case of unbalanced magnetron

* Corresponding author. Tel.: +86 23 65111279; fax: +86 23 65111279.
E-mail addresses: yjshi001@yahoo.com.cn (Y. Shi), siyuan_long@yahoo.com (S. Long).

0169-4332/$ – see front matter © 2009 Elsevier B.V. All rights reserved.
doi:10.1016/j.apsusc.2009.02.044

sputtering, Kelly and Arneli proposed a novel structure zone model [13].

In recent years, the growth of sputtering coatings has been the focus of many theoretical and experimental works. For the stable growth of thin coating, three basic modes have been proposed, including the layer-by-layer mode, island growth mode and layer-plus-island mode on the monocrystal substrate. The columnar growth is an ordinary model for polycrystalline and amorphous coatings, and the theory of ballistic aggregation represented the evolution progress of columnar microstructure [14]. The process governing morphological evolution of thin coating can be developed via research of the surface dynamics at the atomic scale. Most of sputtering deposition on a polycrystalline substrate and the deposition process was an unstable growth due to the rapid deposition rate [15]. During the growth of coatings, the self-shadow, the local curvature, interfacial temperature, diffusion and revised tangent rule played an important role through deposition process [16–19]. The scaling theory depicted the ordinary interface motion property of thin coating [20,21], and the grass model emphasized the effect of shadowing and diffusion on thin coating growth [22]. For thicker coating growth, abundant ion impingement can affect the coating deposition and evolution of surface profile, so surface diffusion must be affected by the ion-to-atom arrival ratio and pulsed flux [23,24].

In the present work, the CrN_x ($0 < x = N/Cr < 1$, atomic ratio) coatings of different composition and thickness were prepared by DC reactive planar magnetron sputtering, and the effect of N_2 content and thickness on the CrN_x coatings on Mg alloy was characterized by XPS, XRD, FESEM and Scanning Probe Microscope (CSPM). The effects of N_2 content and thickness on morphologies evolution were discussed, and the detailed research results are described below.

2. Experiment details

A series of CrN_x coatings were prepared on AZ31 Mg alloy by the planar DC reactive magnetron sputtering system. The vacuum system with internal size Φ450 mm × H300 mm is a single wall of stainless steel cylinder, and the cape hood can be elevated by lifting arm. A 2XZ-8 type backing vacuum sliding vane rotary pump and a FB600 type turbo molecular pump composes vacuum pumping system. A 2 kW direct current power and 2 kW direct current bias voltage power compose supplies system. A FP93 type heating power was used to control workpiece temperature, which ranged from room temperature to 300 °C and the heating source was a heating wire fixed at the background of a sample holder. A round planner magnetron with a size of Φ60 mm was water cooled and used to create the deposition gas phase. The sample holder fixed on cape hood faces magnetron, and the distance of substrate-to-target can be adjusted from 30 mm to 100 mm.

The nummular substrates were machined and polished by 6 μm diamond abrasive paper, and then the sample was fixed in sample holder after being ultrasonically cleaned in acetone for 30 min. The CrN_x coatings were deposited in an atmospheric mixture of Ar and N_2 using a metal Cr target with a purity 99.95 at.%. Before depositing, the chamber base pressure was pumped to 7.4×10^{-4} Pa, and then the interface of Mg alloy substrate was pre-sputtered cleaning around 10 min at minimum current after inputting the Ar. Subsequently, N_2 was inputted with different flow rates (standard cubic centimeter per minute). During the deposition step, the distance between substrate and target was 70 mm. To improve the adhesion force, a metallic Cr adhesive layer of about 150–200 nm thick was deposited prior to the deposition of the normal CrN_x coatings. In order to discuss the effect of nitrogen content $\varphi(N_2)$ and thickness on the CrN_x coatings, the CrN_x coatings have been prepared under various N_2 content and deposition time conditions. The main technological parameters are shown in Table 1.

A Nova400 type FESEM was used to observe the surface and cross-section morphologies of CrN_x coatings. The chemical state of CrN_x coatings was checked by an ESCALAB 250 type XPS. The analyzer was operated by a monochromator in the constant analyzer energy (CAE), Al Kα source (1486.84 eV) radiation and large area XL lens mode, the energy step size at 0.1 eV and the pass energy at 50 eV. The calibration of the binding energy scale was performed according to a standard procedure and the following standards: $Au4f_{7/2}$ (84.0 eV), $Ag3d_{5/2}$ (368.3 eV) and $Cu2p_{3/2}$ (932.7 eV). The thickness of CrN_x coatings was measured by a ball crater and a measuring scale of FESEM. The evaluation of the phase of CrN_x coatings was analyzed by a high resolution Rigaku D/Max-2500 type XRD instrument with a thin coating attachment (a glancing angle mode), Cu Kα radiation and generator settings of 40 kV and 30 mA. The composition of CrN_x coatings was analyzed by XPS and X-ray energy dispersive spectrum (XEDS). The X-ray spectrums were acquired in a continuous mode with 2θ single scanning, a step size at 0.02°, scanning speed at 6°/min, and the grazing incident angle at 2°. The surface roughness and grain size distribution were analyzed by a CSPM5000 type, which was operated at atomic force microscope (AFM) mode. The grain size distributions were taken from different regions at contact mode by a monocrystalline silicon probe with 7 nm radius of curvature.

3. Results

3.1. The effect of N_2 content on CrN_x coatings

The CrN_x coatings on AZ31 Mg alloy were prepared at different $\varphi(N_2)$ and deposition time that were used to control coating composition and thickness. The measured substrate temperature given in Table 1 indicates that substrate temperature increases with the increase in $\varphi(N_2)$. At the same time sputtering power increase conformably resulting in temperature increase. The effect of $\varphi(N_2)$ on the composition is given in Fig. 1, which indicates that the relative concentration of N atom in CrN_x coatings presents exponential growth with the increase in $\varphi(N_2)$. During magnetron sputtering, combination reaction is present on growing interface,

Table 1
Deposition parameters of CrN_x films by planner magnetron sputtering.

	Sample no.											
	1#	2#	3#	4#	5#	6#	7#	8#	9#	10#	11#	12#
N_2 content	0	5%	10%	12.5%	15%	20%	25%	31%	28.6%	28.6%	28.6%	28.6%
Target power (W)	84	93	99	115	120	126	144	156	105	105	105	105
Bias voltage (V)	−100	−100	−100	−100	−100	−100	−100	−100	−100	−100	−100	−100
Total pressure (Pa)	0.5	2.6	2.6	2.6	2.6	2.5	2.6	2.6	2.6	2.6	2.6	2.6
Substrate temperature (°C)[a]		47	45	55		60.5	65.8	66	38	47	54.5	87
Thickness (nm)	2000	1300	1600	1500	2400	1600	1450	1400	300	600	1300	2900

[a] The substrate temperature is not interface temperature but back temperature of sample.

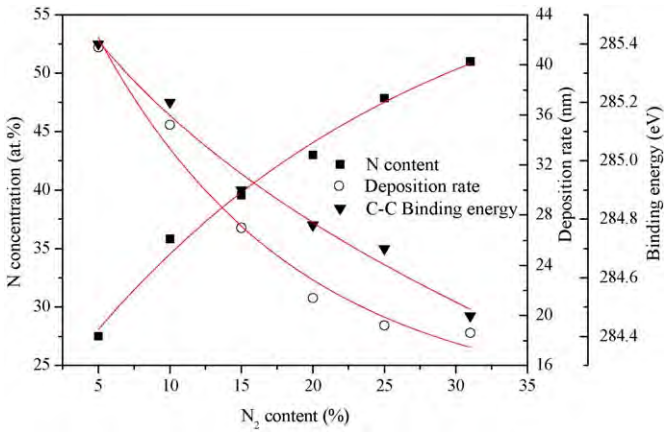

Fig. 1. Effect of N_2 content $\varphi(N_2)$ on N atomic content, binding energy of C–C and deposition rate of CrN_x coatings.

and the reaction should affect the adatom diffusion and growth structure. The relative atomic concentration is subject to relative atom ratio of reaction materials co-arriving to reaction interface; the increasing N_2 content results in the increase of N atomic adsorptive ratio and interfacial reaction; and as a result the relative concentration of N atom increases. The N concentration analyzed by XPS is lower than XEDS about 5–10%, but the change tendency is consistent.

According to the measured thickness of coatings and deposition time, the corresponding mean deposition rates have been evaluated for different N_2 content. Ball crater and SEM measuring scale were used to check thickness of the group CrN_x coatings, indicating similar results. The effect of N_2 content on the deposition rate is given in Fig. 1, which reveals that deposition rate decreases with the increase in $\varphi(N_2)$; the fitting curve suggests that the deposition rate presents exponential decay. The increase in N_2 content $\varphi(N_2)$ resulted in the increase of coverage area of compound because the sputter yield of compound is lower than that of metal, and as a result the particle flux decreased [25–27]. As a function of N_2 content, the deposition rate demonstrates the exponential decay for most of nitride coatings, such as Zr–N and Ti–N [28,29]. The sticking coefficient is a significant factor on the deposition rate, which decreased with the increase in N_2 content [30]. The sputtering voltage increases with N_2 content, and follows the increase of bombardment ion flux, so the resputtering effect can result in the decrease of sticking coefficient. The interfacial temperature and impinging ion flux of thickening coating increased isochronously and at a certain extent contributed to the decrease of deposition rate.

The chemical state of CrN_x coatings was analyzed by XPS, and the analysis of survey scanning shows the presence of the peaks Cr, N, O and C. In the C1s spectrum, adsorptive carbon and a little carbide (282.6 eV) occur, as given in Fig. 2 (A). The C1s spectrum disappears after the samples have been etched for some minutes, indicating that adsorptive carbon is present on the top of the coatings. The Shirley background subtraction method was used to correct narrow scanning spectrum of various elements, which were fitted by using the Lorentzian–Gaussian function, and the chi-square value has been minimized. The O1s spectrums indicate several oxides are present including Cr_2O_3 (530.35 ± 0.4 eV [31–33]), $Cr(OH)_3$ (531.4 ± 0.4 eV [31,33]), as well as adsorptive oxygen and adsorbed water (532.53 eV and 533.54 eV [34,35]), the peak situated at 529.12 eV may belong to CrO_3 (529.7 eV [35]), as shown in Fig. 2(B). Deconvolution spectrums of N1s reveal that Cr_2N (397.6 eV [36]) and CrN (396.7 eV [37]) are present in CrN_x coatings, as given in Fig. 3. The nitride in coatings is gradually changed into CrN from Cr_2N with the increase in $\varphi(N_2)$, and relevant binding energy gradually

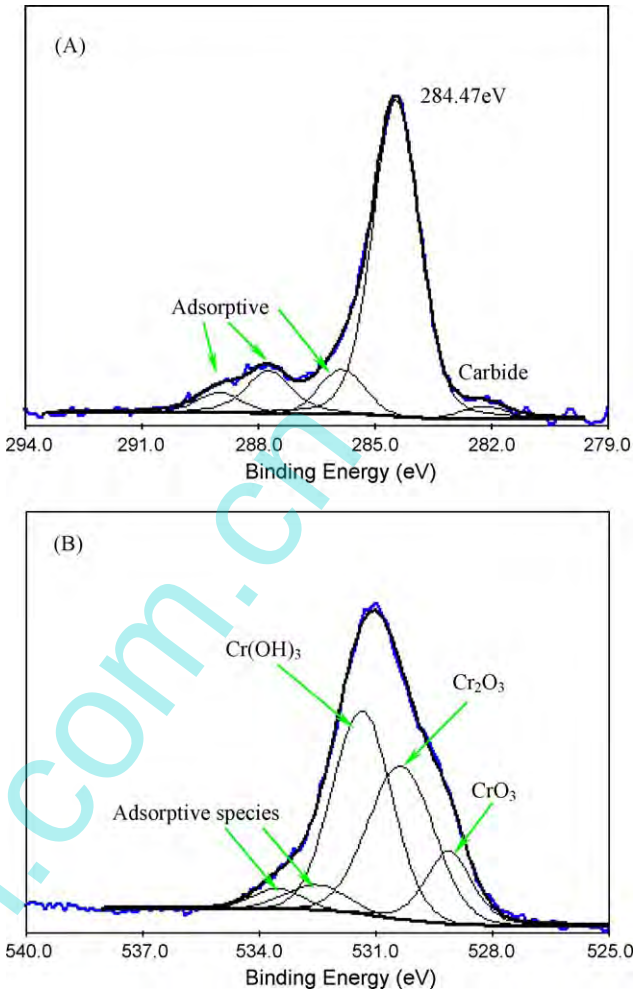

Fig. 2. XPS spectrums of C1s (A) and O1s (B) on surface of CrN coatings, at $\varphi(N_2) = 31\%$.

shifting downward about 1.2 eV. It is rather remarkable that the reference binding energy of C1s (C–C or C–H) presents an exponential decay with the increase in $\varphi(N_2)$, as given in Fig. 1.

The structure evolution of CrN_x coatings is shown in Fig. 4, which reveals the close-packed hexagonal structure when $\varphi(N_2)$ is between 5% and 15%, and the peak intensity increases with the increase in $\varphi(N_2)$; the structure belongs to FCC when the $\varphi(N_2)$ is increased from 20% to 31%. Combined with the composition and chemical state of coatings, the coating phase includes Cr and Cr_2N at $\varphi(N_2) = 5\%$, and the microcrystallite of body-centered cubic (BCC) and HCP structure is intermixed. The Cr_2N phase demonstrates the obvious preferred $(1\,1\,\bar{2}\,1)$ out-plane orientation when $\varphi(N_2)$ increased to 12.5%. The face-centered cubic (FCC) structure occurs at $\varphi(N_2) = 20\%$, and the $(1\,1\,\bar{2}\,1)$ out-plane orientation is changed into (2 0 0) out-plane orientation of FCC structure. For the CrN phase, the (1 1 1) and (2 2 0) orientation intensity gradually increase with the increase in $\varphi(N_2)$, while the (2 0 0) peak intensity gradually decreases. The diffraction peaks of Mg alloy substrate can be found at XRD spectrums, and the diffraction intensity of Mg alloy gradually decreases with the increase in $\varphi(N_2)$, indicating the coatings density increases isochronously with the increase in $\varphi(N_2)$.

The effect of $\varphi(N_2)$ on the growth structure of CrN_x coatings was depicted by fractured cross-section, and surface morphologies were observed by FESEM. Fractured cross-section morphologies of CrN_x coatings are given in Fig. 5, which clearly presents the coatings' growth affected by the $\varphi(N_2)$. For metal Cr coating,

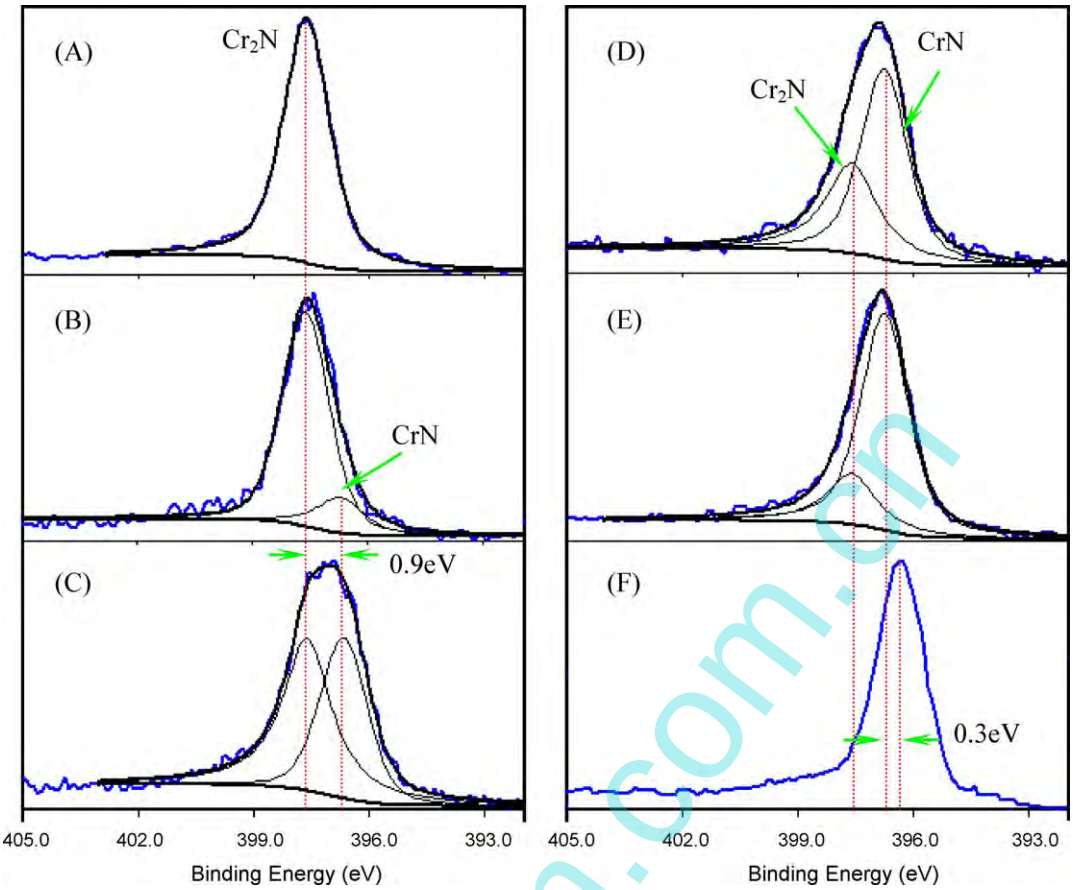

Fig. 3. N1s spectrums of CrN_x coatings with different N_2 contents: (A) $\varphi(N_2) = 5\%$, (B) $\varphi(N_2) = 10\%$, (C) $\varphi(N_2) = 15\%$, (D) $\varphi(N_2) = 20\%$, (E) $\varphi(N_2) = 25\%$ and (F) $\varphi(N_2) = 31\%$.

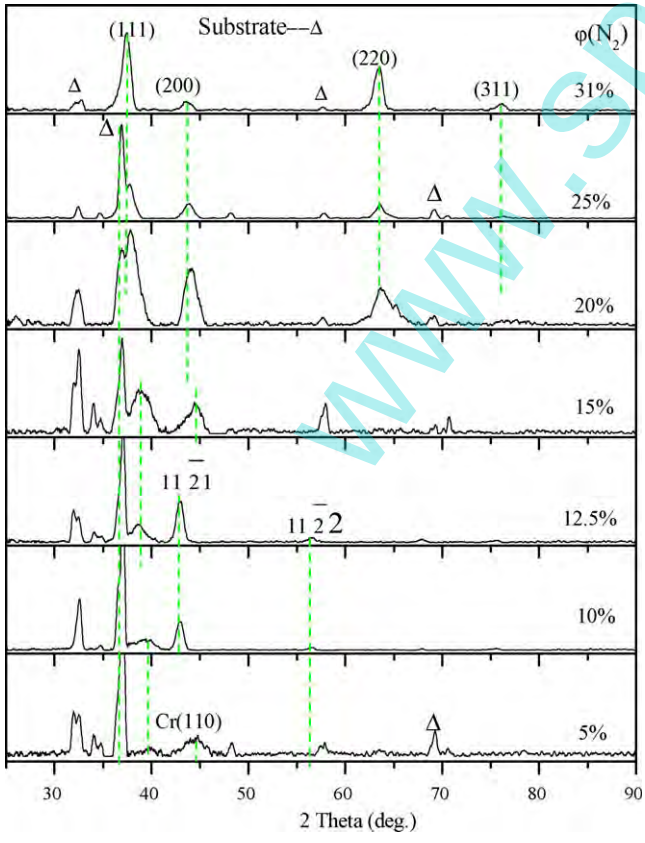

Fig. 4. XRD spectrum of CrN_x with different N_2 contents $\varphi(N_2)$.

morphology reveals that fibre growth belongs to Z1 structure. In $\varphi(N_2) = 5\%$, the growth structure shows that porous appearance is present in fractured cross-section, and the corresponding surface morphology reveals that flocculent structure is made of abundant fibre crystal, as given in Fig. 6. When the $\varphi(N_2)$ increases to 15%, abundant porosity disappears and the density clearly increases, and the leafy surface structure with grooved boundaries occurs. Subsequently, the clear columnar growth can be seen, and the corresponding surface morphology reveals that some bigger granular crystals with cone dome are present. The open boundary between columnar crystals is present when the $\varphi(N_2)$ increases to 31%. The results reveal that the decrease in abundant boundary promotes adatom diffusion. So, an elevated $\varphi(N_2)$ causes intergrain boundaries to become more open, a dense columnar competitive growth is more and more clearly with the increase in $\varphi(N_2)$, although bombardment ion flux increases due to elevated target voltage.

The surface roughness of the CrN_x coatings can be depicted by random three-dimensional thicker profiles, which were analyzed by the CSPM5000, as given in Fig. 7. The Root Mean Square (RMS) roughness of surface profile is defined as [22]

$$W_{\mathrm{RMS}}(L) = \sqrt{\frac{1}{MN}\sum_{j=0}^{M-1}\sum_{k=0}^{N-1}\left[h(x_j, y_k) - h_M\right]^2}, \quad (1)$$

$$h_M = \frac{1}{MN}\sum_{j=0}^{M-1}\sum_{k=0}^{N-1} h(x_j, y_k). \quad (2)$$

In this formula, the $h(x_j, y_k)$ presents coordinates point of three-dimensional profiles, and h_M presents the mean roughness value. The surface roughness W_{RMS} increases exponentially with the increase in $\varphi(N_2)$. For the results, the basic understanding indicates

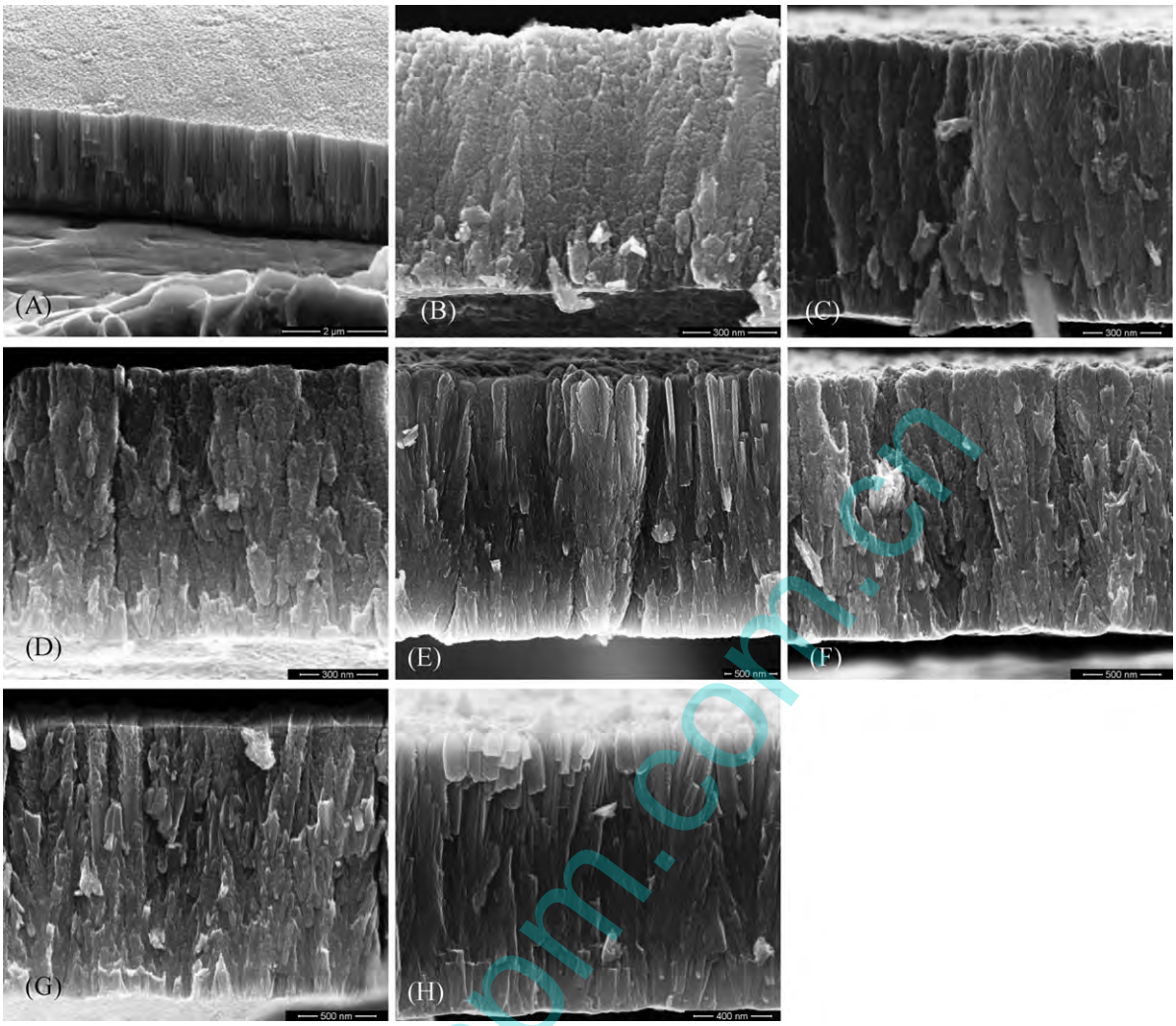

Fig. 5. Fractured cross-section morphologies of CrN_x coatings with different N_2 contents: (A) $\varphi(N_2)$ = 0, (B) $\varphi(N_2)$ = 5%, (C) $\varphi(N_2)$ = 10%, (D) $\varphi(N_2)$ = 12.5%, (E) $\varphi(N_2)$ = 15%, (F) $\varphi(N_2)$ = 20%, (G) $\varphi(N_2)$ = 25% and (H) $\varphi(N_2)$ = 31%.

in-plane grain grows with $\varphi(N_2)$ increasing, and the maximum height h^* increases synchronously, so W_{RMS} increases. In three-dimensional profiles, the higher peaks present columnar crystal with predominance and the lower peaks present columnar crystal in inferior position.

3.2. The effect of thickness on properties of CrN coatings

The CrN coatings with different thickness deposited at different deposition times, and corresponding parameters are shown in Table 1, composition and chemical state of the group samples are given in Figs. 1 and 3. The measuring substrate temperature increases from 35 °C to 87 °C with the increase in coatings' thickness. The deposition process of CrN coatings can be pictured as occurring in three steps followed by deposition of Cr adhesive layer, transition layer and normal chemical compound layer. The effect of coatings' thickness on grain-orientation evolution of CrN coatings deposited at low sputtering power is given in Fig. 8. The out-plane Cr(1 1 0) is present at h = 300 nm, as well as out-plane (1 1 1) and (2 2 0) of FCC structure, while the Cr(1 1 0) peak disappears when the coatings' thickness increases to 600 nm. The diffraction intensity of FCC structure increases with the increase in coatings' thickness h. In comparison with powder diffraction of similar composition, an obvious (2 2 0) and (1 1 1) are present at XRD spectrums. The texture orientation of thick coatings should be affected by initial growth orientation, and the grain growth shows that the texture orientation develops with the thickening of coating.

The in-plane mean grain size of CrN coatings can be defined as A_t/N, where the A_t and N present in-plane total area and total grain number, respectively. The in-plane grain size d_{ia} can be defined as $(4A/\pi)^{1/2}$, where the A presents in-plane grain area. The fractured cross-section morphologies and surface morphologies of CrN coatings with different thickness are shown in Figs. 9 and 10, which present the in-plane diameter d_{ia} and height of columnar crystal h through thickness increase. The top of CrN coatings presents trigone cone dome, which suggests lower ion impingement to the growing interface. The columnar crystal acquires a bigger development through the deposited thickness during adhesive layer step depositing, and the growth mode continues with h thickening. The density of coatings' bottom increases with the increase in thickness due to secondary growth of grain. Elevated deposition temperature and compressive stress are responsible for the secondary growth [38].

The d_{ia} is direct ratio to the h, as shown in Fig. 11. The in-plane mean grain size d_{ia} increases with the thickening of coatings that can be depicted by the following formula [39]:

$$d_{ia} = \alpha t_D{}^n + d_0 \approx d_{01} + k'h, \quad (3)$$

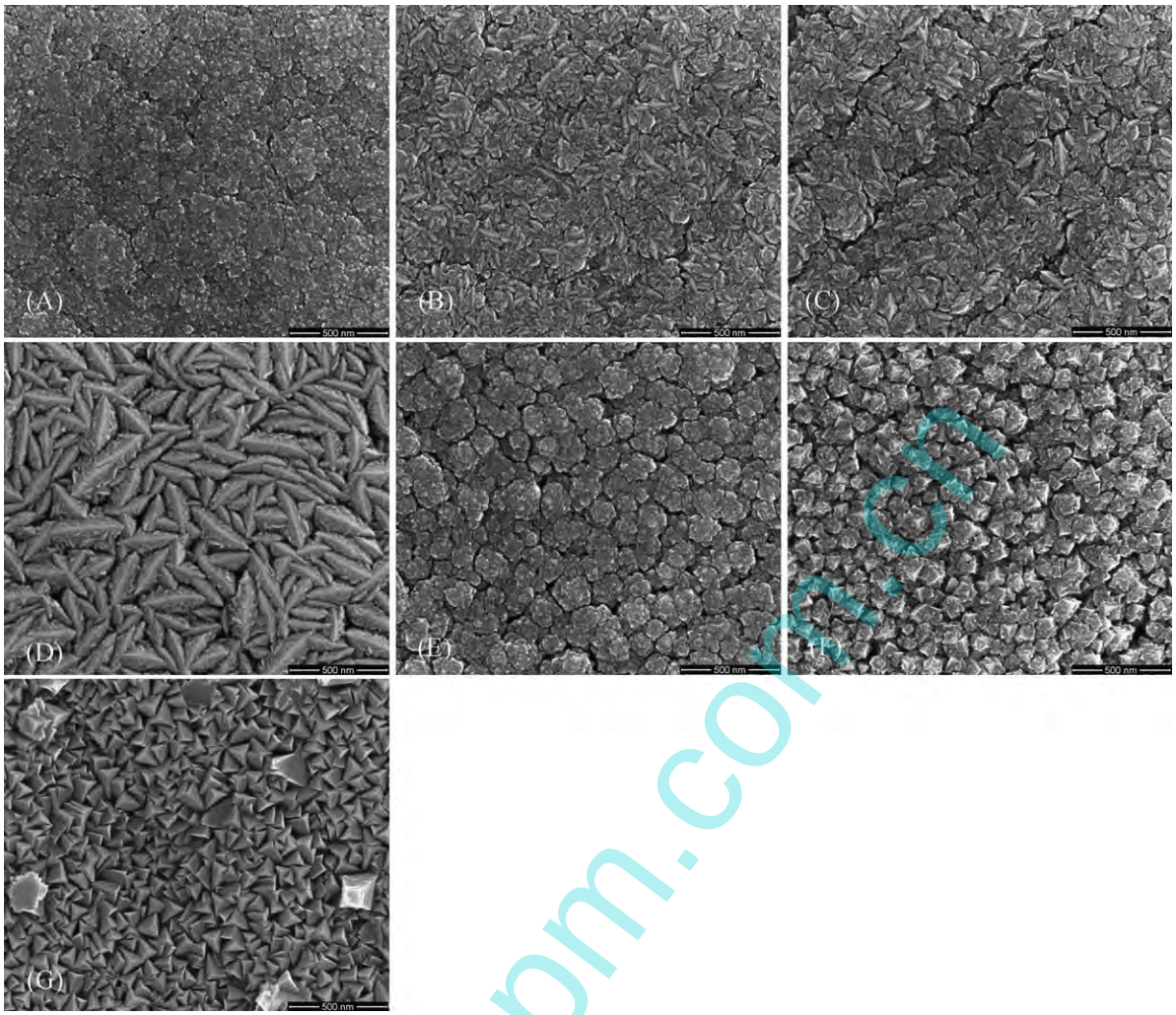

Fig. 6. Surface morphologies of CrN_x coatings with different N_2 contents: (A) $\varphi(N_2)$ = 5%, (B) $\varphi(N_2)$ = 10%, (C) $\varphi(N_2)$ = 12.5%, (D) $\varphi(N_2)$ = 15%, (E) $\varphi(N_2)$ = 20%, (F) $\varphi(N_2)$ = 25% and (G) $\varphi(N_2)$ = 31%.

where a and k' are thermally activated kinetic rate constants, t_D is the deposition time, d_0 and d_{01} are the average initial in-plane diameter, and n expresses the exponent related with grain growth activation energy. In this formula, n is 1, indicating the mean value. Actually, n values for the different cones are assumed to have a Gaussian distribution centered about value n_0 with a standard deviation σ. Lita et al. researched the growth property of metal Al coating [42], indicating that the n is 0.9. The out-plane grain size of coatings d_{oa} is larger than in-plane grain size (d_{ia}). The distribution of in-plane grain size belongs to normal distribution, which suggests the presence of competitive growth. Under annealing conditions, the in-plane average grain growth governed by time and temperature should obey the revised parabolic kinetics in thin coating [40].

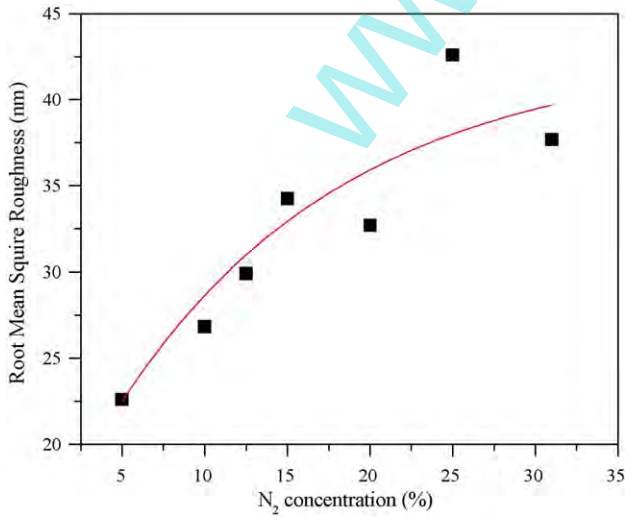

Fig. 7. The effect of N_2 content on surface roughness W_{RMS}.

Correspondingly, it is found that W_{RMS} increases monotonically with the increase in h and demonstrates property of power function, as shown in Fig. 11. The W_{RMS} values which were acquired by the CSPM5000 have similar change tendency with digitized SEM images. The results indicate that the amplitude of vibration gradually increases and the surface roughness W_{RMS} presents growth of exponential function with the increase in h, and the formula can be expressed as follows:

$$R_{RMS} \approx P_1 h^a. \quad (4)$$

In this formula, a value is 0.7589 and P_1 is 0.0801, and the correlation coefficient of regression line R^2 = 0.99948 and variance χ^2/DoF = 0.0969. The thickness h is a function of time t, so W_{RMS} can be expressed as $W_{RMS}(L,t) \sim t^{\beta}$ (for $t/L^z \ll 1$), where β presents the temporal growth exponent [41]. This is the result of anisotropy of grain growth during coating thickening. Actually, the enlarged

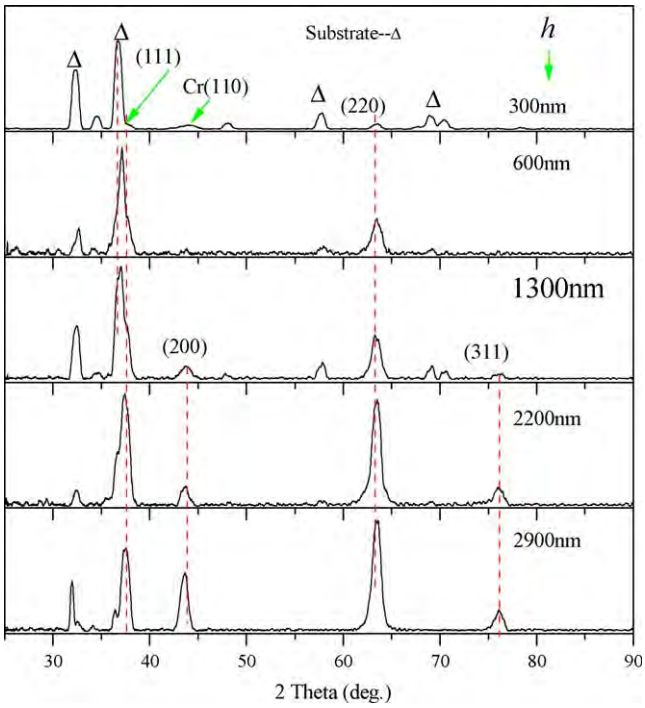

Fig. 8. XRD spectrums of CrN coatings with different thicknesses h_t.

in-plane diameter accounts for the increase in maximum height, so the surface roughness increases.

The in-plane grain size distributions were determined by the CSPM5000 which was operated at AFM mode, as shown in Fig. 12. The different region was scanned until the recorded grain was no less than 400. In comparison with average equivalent diameter by SEM images, the calculated diameter is consistent. The normal distribution curve was acquired from average value of original data and sample standard deviation, and the counts intensity occurs during statistics and corresponds to the percentage of grain size distribution. The normal distribution curve is expressed as follows:

$$f(d) = \frac{1}{\sigma\sqrt{2\pi}} e^{(d-d_{ia})^2/\sigma^2}. \quad (5)$$

The σ presents standard deviation of $d - d_{ia}$. In this formula, σ and d_{ia} are independent of each other. The distribution space of grain size increases with the increase in h, and the corresponding sample variance σ^2 increases synchronously. The d_{ia} increases with thickening of coating, and a significant shift in the distribution also can be seen. The Gaussian distribution curve of in-plane diameters characters growth property of grain coating, anisotropic property and competitive growth are the intrinsic reasons. The grains with competitive predominance continue to grow up, and the grains which are in inferior position are shadowed and coalesced, which suggests that coarsening mechanism of texture evolution contains shadow and coalescence during thickening.

The statistic variance σ^2 of CrN coatings is given in Fig. 13, which reveals that variance increases linearly with the increase in thickness. The fitted regression line is as follows:

$$\sigma^2 = -183.05 + 1.2708h. \quad (6)$$

For the fit formula, related coefficient $R = 0.99738$ and standard difference SD = 131.21. On the assumption that $\sigma^2 = 0$, a critical thickness value can be acquired at $h = 144$ nm. The result shows that a critical thickness may occur during the thickening of CrN coatings, and competitive columnar growth occurs after h exceeds

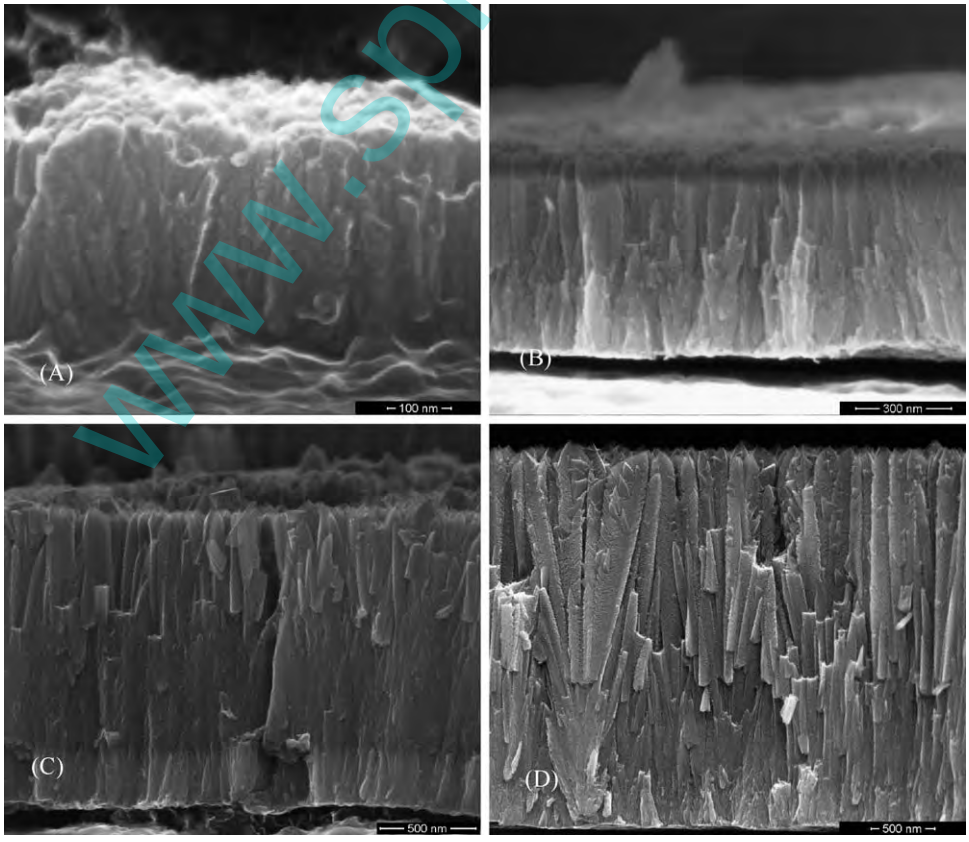

Fig. 9. Fractured cross-section morphologies of CrN coatings with different thicknesses: (A) $h = 300$ nm, (B) $h = 600$ nm, (C) $h = 1300$ nm and (D) $h = 2900$ nm.

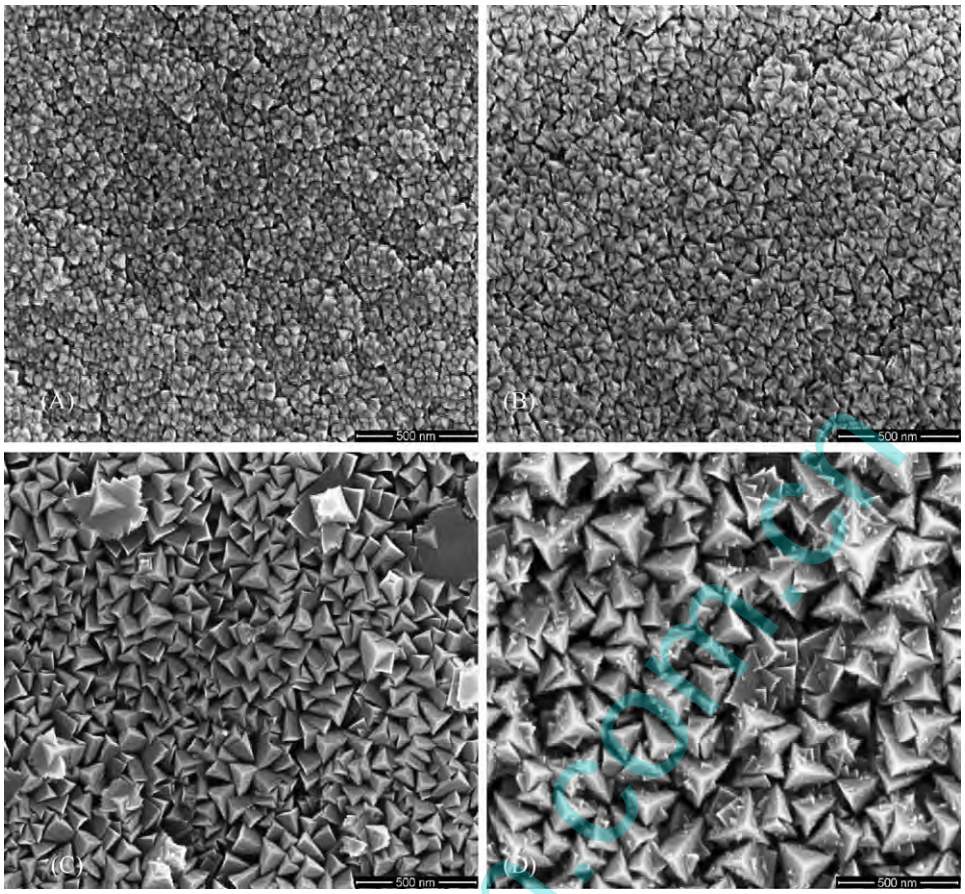

Fig. 10. Surface morphologies of CrN coatings with different thicknesses: (A) h = 300 nm, (B) h = 600 nm, (C) h = 1300 nm and (D) h = 2900 nm.

critical thickness value, but columnar crystal d_{ia} is adjacent to critical thickness value.

4. Discussion

The composition of coatings is mainly subject to reactive gas concentration and sputtering power and the deposition temperature. Furthermore reactive rate of interface and the reaction coefficient do still have an effect on composition. For the coatings with solid solution or interstitial phase, atomic relative concentration can change in a finite range, while the structure and phase content can stabilize, and the typical magnetron sputtering process satisfies the condition. During depositing, effective reaction occurred on thickening interface due to higher deposition rate. Several reactive sputtering models depicted the essential deposition process, such as Hofmann model [43], Berg model and Shinoki model [44,45]. If N_2 content can stabilize, the Ar^+ ions flux J_{Ar^+} present linear or exponential growth with increase in discharge current I_{Ar} [46]. If discharge current can stabilize, the N_2^+ and N^+ ion flux J_{N^+} present exponential growth with increase in partial pressure, while ions flux J_{Ar^+} is unchanged [45]. So, the ions flux J_{N^+} increases with increase in N_2 content, indicating an increase in N atomic concentration. As a N_2 content function, the change of N atomic concentration is consistent with deposition rate, and follows the change of growth structure. The results of XPS and XRD are consistent, indicating that the N atomic concentration governs the structure evolution.

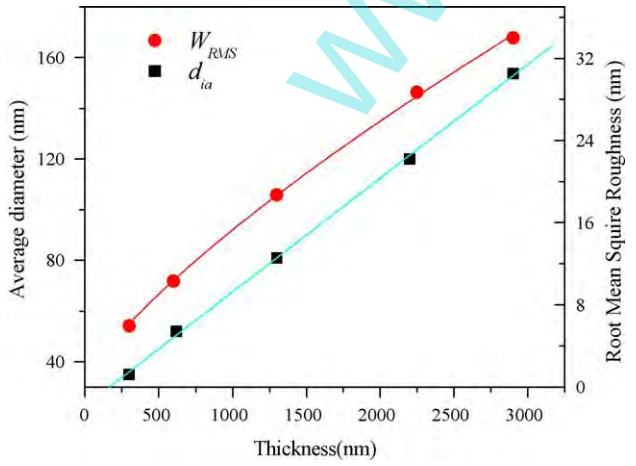

Fig. 11. Effect of thickness on in-plane grain size and surface Root Mean Square roughness.

The combination of Figs. 5 and 6 suggest that growth structure of CrN_x coatings is subject to x (N/Cr) and phase, zone structure gradually changes from fibre to columnar growth. A novel structure zone model is summarized to describe the effect of x (N/Cr) on observed structure and phase variation, and the model is shown in Fig. 14, indicating that the structure changes from Z1 into Z2 with the increase in x. Note that Z3 structure has not been included. When the atomic ratio of N/Cr is $0 < x < 0.4$, the structure of CrN_x coatings belongs to Z1, which corresponds to $Cr + Cr_2N$. When the atomic ratio of N/Cr is $0.4 < x < 0.5$ and $0.7 < x < 0.8$, the structure of CrN_x coatings belongs to ZT (transition zone), which corresponds to $Cr_2N + Cr$ and $CrN + Cr_2N$, respectively. The ZT with $CrN + Cr_2N$ presents columnar growth, which belongs to sub-ZT due to obscure boundaries, and an anomalous W_{RMS} occurs in the region. When the atomic ratio of N/

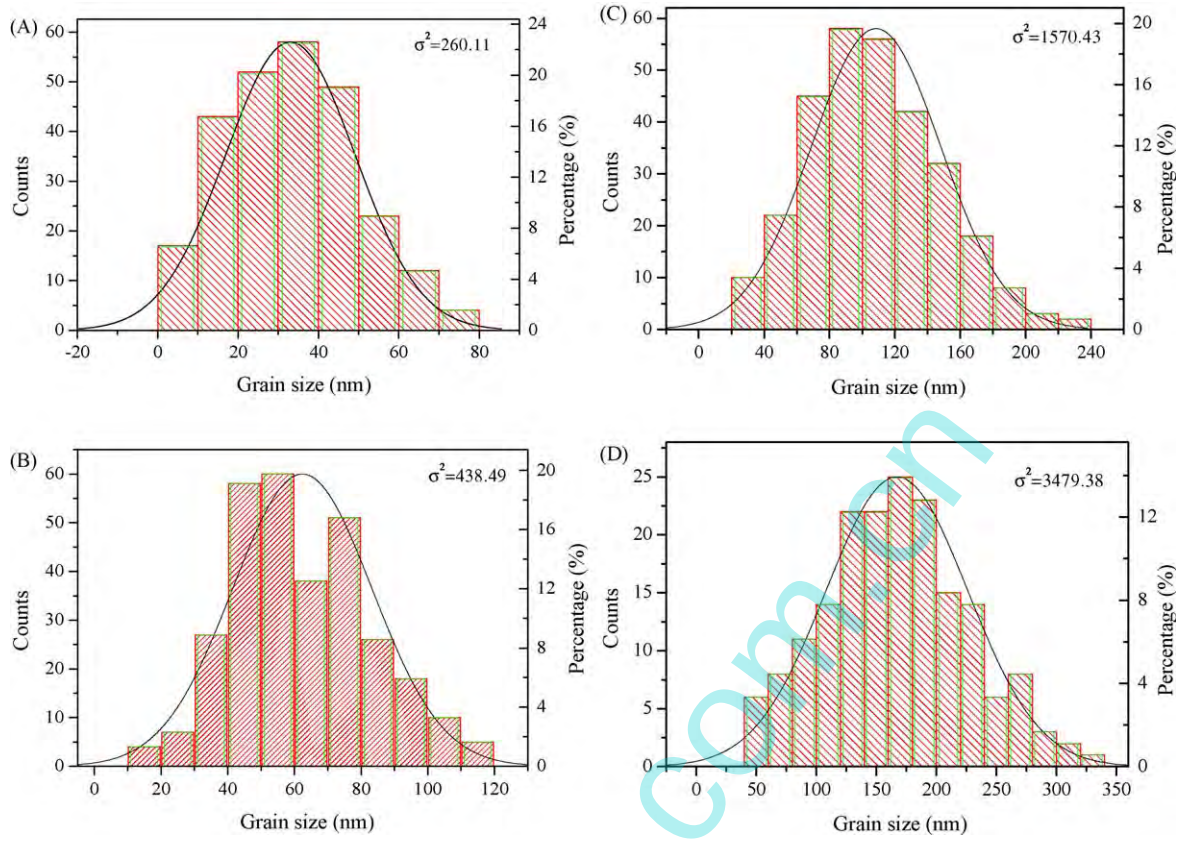

Fig. 12. Grain size distribution analyzed by CSPM with different thicknesses: (A) h = 300 nm, (B) h = 600 nm, (C) h = 1300 nm and (D) h = 2900 nm.

Cr is $0.5 < x < 0.7$ and $x > 0.9$, the Z2 structure occurs, indicating the open columnar crystal boundaries, which corresponds to CPH and FCC structure. The SZM indicates that the self-shadow effect and diffusion govern the growth structure under limited ion impingement conditions and result in the presence of porosity appearance.

Moreover, our research reveals that the relationship of deposition rate vs. coatings' thickness presents three-step of change of deposition rate: adhesive layer, transitional layer and normal chemical composition. The deposition rate of adhesive layer increased with the increase in target current, and sputtering mode promptly changed from metal mode into compound mode with the inputting of reactive gas, as a result the deposition rate decreased. For the deposition of normal composition coatings, the deposition rate presents exponential decrease in thickening of coatings; it is the possible reason that the decrease of the crystal face condensation probabilities results in decrease of adsorption site due to competitive columnar growth. During sputtering deposition, the coverage area of compound on surface of cathode target is varying with ion flux bombardment continuing, and as a result of uneven ion distribution and fluctuation of J_{N^+} content. With the increase in sputtering current, the deposition rate increases, at the same time the elevating of deposition temperature is followed due to adatom condensation and ion bombardment. Furthermore, the stress is still an un-neglected factor, and it is developed with the thickening of coatings, so that the sticking coefficient decreases.

Figs. 8–10 demonstrate that the evolution process of structure and orientation of the CrN coating, and the columnar growth and orientation develop with the thickening of coating, although the out-plane growth is affected by the chemical bond in transitional layer. According to the structure zone model, growth structure of CrN coating belongs to Z2, and adatom diffusion is sufficient to overcome self-shadowing effect. The deposition temperature

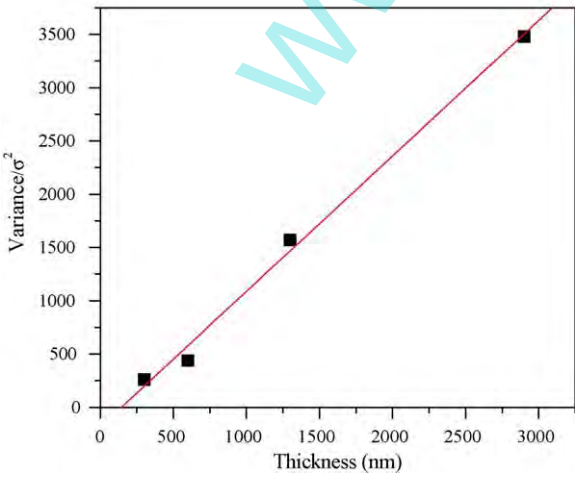

Fig. 13. Relationship between statistic variance of grain distribution and thickness.

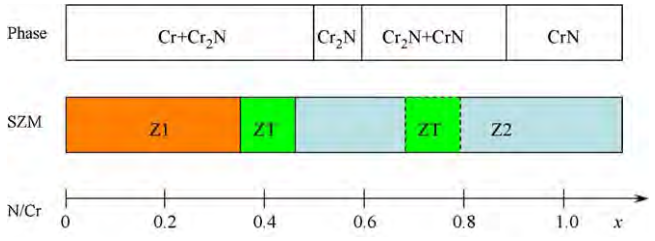

Fig. 14. Evolution of structure zone and phase for CrN_x coatings described by reactive DC magnetron sputtering.

increases with the thickening of coating, and provides driving force for secondary growth on bottom of thickening coating. In this case, the adhesive property should change with coating thickening. The evolution of surface profile and W_{RMS} presents the critical height at local region obeys the distribution of power function, surface free energy and deposition rate account for the result. The variance grain size distribution σ^2 increases with the increase in thickness, and indicates that the columnar crystal with competitive advantage develops synchronously.

During the thickening of coating, the columns' number and crystal boundaries' number unit area are significant factors. The abundant boundaries between columns with different structure constrict the adatom diffusion and hold back the in-plane grains growing. In general, columns' number unit area decrease with the increase in $\varphi(N_2)$, as a result the diffusion constant D increases. Moreover, deposition rate R decreases with the increase in N_2 content, and the D/R presents exponential growth. It is possible that KBR model can provide an explanation of the above-mentioned structure evolution [16]. In this growth case, the growth is terminated or the deposition rate R is sharply reduced, once the h reaches the critical height, which increases with the increase in $\varphi(N_2)$; so the resulting increase in W_{RMS} occurs. The self-shadow effect and anisotropic property govern the adatom diffusion; in-plane grain grows with the thickening of coating, following that the boundaries and columns decrease. The adatom diffusion is limited by the surface tension and anisotropic surface energy with the thickening of coating; the lattice mismatch and minimization of crystal face energy may have an effect on adatom diffusion [47,48].

5. Conclusion

The CrN_x coatings on Mg alloy substrates were prepared by DC reactive planar magnetron sputtering at a mixed atmosphere containing Ar and N_2. The effects of N_2 content and thickness on the CrN_x coatings were characterized by the XPS, XRD, FESEM and CSPM, respectively. The N atomic concentration increased with the increase in N_2 content, and the corresponding binding energy of N1s shifts downward about 1.2 eV. At the same time the structure changes from HCP structure into FCC structure. The growth structure of CrN_x coatings develops from fibre growth to columnar growth, and gradually forms open boundary; the deposition rate decreases exponentially with the increase in N_2 content. Based on the evolution of phase and structure, a SZM model is summarized, indicating that the change of structure and phase is consistent; ZT and sub-ZT correspond to $Cr_2N + Cr$ and $CrN + Cr_2N$, respectively. The surface Root Mean Square roughness W_{RMS} increases exponentially with the thickening of coating, and grain size obeys normal distribution.

Acknowledgments

In the present work, some helpful advice was acquired from Dr. Weiqing Wang, Dr. Liping Peng, Jianxin Dong and Yong Chen for sample preparation, and sample analysis was supported by Dr. Jianwei Chen, Tianlin Huang, and Chunhua Wang, the author sincerely thanks them for assistance of the present work.

References

[1] H. Altun, S. Sen, Surface & Coatings Technology 197 (2005) 193–200.
[2] F. Hollstein, R. Wiedemann, J. Scholz, Surface & Coatings Technology 162 (2003) 261–268.
[3] Y. Shi, S. Long, L. Fang, S. Yang, F. Pan, Applied Surface Science 254 (2008) 5861–5867.
[4] Y. Shi, S. Long, S. Yang, F. Pan, Applied Surface Science 254 (2008) 7342–7350.
[5] K.H. Nam, M.J. Jung, J.G. Han, Surface & Coatings Technology 131 (2000) 222–227.
[6] J.A. Sue, T.P. Chang, Surface & Coatings Technology 76–77 (1995) 61.
[7] C. Liu, A. Leyland, S. Lyon, A. Mathews, Surface & Coatings Technology 77 (1995) 623.
[8] P. Hones, R. Sanjinés, F. Lévy, Surface & Coatings Technology 94/95 (1997) 398–402.
[9] C. Rebholz, H. Ziegele, A. Leyland, A. Matthews, Surface & coatings Technology 115 (1999) 222–229.
[10] J.A. Thornton, Journal of Vacuum Science & Technology 11 (1974) 666–670.
[11] J.A. Thornton, Annual Review of Materials Science 7 (1977) 239–260.
[12] P.J. Kelly, R.D. Arneli, Journal of Vacuum Science & Technology: A 19 (1999) 945–953.
[13] P.J. Kelly, R.D. Arneli, Journal of Vacuum Science & Technology: A 16 (1998) 2858–2869.
[14] P. Ramanlal, L.M. Sander, Physical Review Letters 54 (1985) 1828–1831.
[15] R. Bruinsma, G. Aeppli, Physical Review Letters 52 (1984) 1547–1550.
[16] R.P.U. Karunasiri, R. Bruinsma, J. Rudnick, Physical Review Letters 62 (1989) 788–790.
[17] P. Keblinski, A. Maritan, F. Toigo, R. Messier, J. Banavar, Physical Review: E 53 (1996) 759–778.
[18] J.L. Zubimendi, M.E. Vela, R.C. Salvarezza, L. Vázquez, J.M. Vara, A.J. Arvia, Physical Review: E 50 (1994) 1367–1371.
[19] M. Kardar, G. Parisi, Y. Zhang, Physical Review Letters 56 (1986) 889–892.
[20] G.S. Bales, A. Zangwill, Physical Review Letters 63 (1989) 692.
[21] C. Tang, S. Alexander, R. Bruisma, Physical Review Letters 64 (1990) 772–775.
[22] G.S. Bales, R. Bruinsma, E.A. Eklund, R.P.U. Karunasiri, J. Rudnick, A. Zangwill, Science 249 (1990) 264–268.
[23] P.J. Kelly, R.D. Arneli, Journal of Vacuum Science & Technology: A 16 (1998) 2858–2868.
[24] E. Kelesoglu, C. Mitterer, M.K. Kazmanli, M. Ürgen, Surface & Coatings Technology 116–119 (1999) 133–140.
[25] G.A. Zhang, P.X. Yan, P. Wang, Y.M. Chen, J.Y. Zhang, Materials Science and Engineering: A 460–461 (2007) 301–305.
[26] J.-E. Sundgren, B.-O. Johansson, S.-E. Karlsson, Surface Science 128 (1983) 265–280.
[27] Z. Han, J. Tian, Q. Lai, X. Yu, G. Li., Surface & Coatings Technology 162 (2003) 189–193.
[28] R. Mientus, K. Ellmer, Surface & Coatings Technology 116–119 (1999) 1093–1101.
[29] H.A. Jehn, J. Kim, S. Hofmann, Surface & Coatings Technology 36 (1988) 715–727.
[30] D. Mao, J. Hopwood, Journal of Applied Physics 96 (2004) 820–828.
[31] I. Milošev, H.-H. Strehblow, B. Navinšek, M. Metikoš-Huković, Surface and Interface Analysis 23 (1995) 529–539.
[32] M.J. Goldberg, J.G. Clabes, C.A. Kovac, Journal of Vacuum Science & Technology: A 6 (1988) 991–996.
[33] B. Stypula, J. Stoch, Corrosion Science 36 (1994) 2159–2167.
[34] P.-Y. Jouan, M.-C. Peignon, Ch. Cardinaud, G. Lempérière, Applied Surface Science 68 (1993) 595–603.
[35] A. Lippitz, Th. Hübert, Surface & Coatings Technology 200 (2005) 250–253.
[36] P. Marcus, M.E. Bussell, Applied Surface Science 59 (1992) 7–21.
[37] I.L. Singer, J.S. Murday, Journal of Vacuum Science & Technology 17 (1980) 1.
[38] F. Lai, L. Lin, Z. Huang, R. Gai, Y. Qu., Applied Surface Science 253 (2006) 1801–1805.
[39] A. Mazor, D.J. Srolovitz, P.S. Hagan, B.G. Bukiet, Physical Review Letters 60 (1988) 424–427.
[40] J.E. Palmer, C.V. Thompson, H.I. Smith, Journal of Applied Physics 62 (1987) 2492–2497.
[41] A.E. Lita, E. John, Sanchez Jr., Physical Review: B 61 (2000) 7692–7699.
[42] A.E. Lita, E. John, Sanchez Jr., Journal of Applied Physics 85 (1999) 876–882.
[43] S. Hofmann, Thin Solid Films 476 (1990) 335–348.
[44] S. Berg, T. Nyberg, Thin Solid Films 476 (2005) 215–230.
[45] F. Shinoki, A. Itoh, Journal of Applied Physics 46 (1975) 3381–3384.
[46] V.Yu. Kulikovsky, Surface & Coatings Technology 94–95 (1997) 428–432.
[47] C.V. Thompson, Annual Review of Materials Science 20 (1990) 239–268.
[48] C.V. Thompson, Journal of Materials Research 14 (1999) 3164–3168.